

Lawrence Berkeley National Laboratory

LBL Publications

Title

Thermo-Hydro-Mechanical Modeling of Brine Migration in a Heated Borehole Test in Bedded Salt

Permalink

<https://escholarship.org/uc/item/81r3v5wp>

Authors

Tounsi, Hafssa

Rutqvist, Jonny

Hu, Mengsu

et al.

Publication Date

2023

DOI

10.1007/s00603-023-03632-5

Copyright Information

This work is made available under the terms of a Creative Commons Attribution License, available at <https://creativecommons.org/licenses/by/4.0/>

Peer reviewed



Thermo-Hydro-Mechanical Modeling of Brine Migration in a Heated Borehole Test in Bedded Salt

Hafssa Tounsi¹ · Jonny Rutqvist¹ · Mengsu Hu¹ · Kristopher Kuhlman²

Received: 2 July 2023 / Accepted: 15 October 2023
© The Author(s) 2023

Abstract

This research paper focuses on the thermo-hydro-mechanical (THM) modeling of brine migration in a heated borehole test conducted as part of the ongoing Brine Availability Test in Salt (BATS) at the Waste Isolation Pilot Plant (WIPP) in New Mexico. It is a component of the international collaboration project DECOVALEX-2023 (DEvelopment of COupled models and their VALidation against EXperiments), which aims to understand the THM processes governing brine flow in heated rock salt repositories through collaborative analysis by multiple research teams. Using the TOUGH–FLAC simulator, THM simulations were performed and compared with data from the BATS phase 1a. This experiment involved two identical horizontal-borehole arrays, one heated and one serving as a control, both equipped with sensor arrays. Analysis of measurements revealed water flow rate surges during heater power transitions, with the highest jump observed during cooling. Acoustic emission activity exhibited distinct patterns in response to heater power changes, suggesting that damage to rock salt is particularly pronounced during the cooling phase. The THM simulations successfully captured these phenomena, highlighting the significance of thermal effects, brine migration, and mechanical behavior in predicting brine availability in heated and damaged rock salt. Our modeling also revealed the critical interplay between heating and cooling-induced damage and its influence on flow properties, particularly affecting brine inflow estimation. Notably, we found that cooling-induced brine inflow spikes result from increased permeability due to tensile dilatancy. These findings have important implications for the development of robust containment strategies and enhance our understanding of the complex processes involved in repository performance.

Highlights

- Numerical modeling study accurately replicates the thermal-hydromechanical behavior of rock salt surrounding a heated borehole.
- Jumps in brine flow rate during transitions in heater power are observed, with the highest jump during cooling.
- Acoustic emission patterns suggest pronounced damage to rock salt during the cooling phase.
- Thermal pressurization and tensile-induced damage are identified as the primary contributors to brine inflow spikes.
- Findings improve predictions of brine availability, aiding the development of robust containment strategies for radioactive waste disposal.

Keywords Numerical modeling · THM coupling · Rock salt · Brine availability · Heated borehole experiment · Cooling damage

✉ Hafssa Tounsi
htounsi@lbl.gov

Jonny Rutqvist
jrutqvist@lbl.gov

Mengsu Hu
mengsuhu@lbl.gov

Kristopher Kuhlman
klkuhlm@sandia.gov

¹ Energy Geosciences Division, Lawrence Berkeley National Laboratory, Berkeley 94720, Ca, USA

² Nuclear Waste Disposal Research & Analysis Department, Sandia National Laboratory, Albuquerque, NM, USA

1 Introduction

The safe and effective disposal of heat-emitting radioactive waste is of utmost importance, leading to the need for reliable geological repositories for long-term containment. Among the potential host rocks, undisturbed rock salt has gained significant attention due to its ultra-low permeability and porosity, high thermal conductivity, and self-sealing capacity, making it an excellent natural barrier for confining hazardous materials (Sweet and McCreight 1983; Cosenza et al. 1999; Winterle et al. 2012; Chen et al. 2013). However, it is important to recognize that rock salt is not completely devoid of water. Water exists within the salt in various forms but lacks the ability to circulate freely.

Excavation activities associated with mining underground rooms or boreholes can induce fractures in the salt formation, creating a damaged rock zone around the excavated structures. Consequently, the presence of brine in the vicinity of the excavation becomes a concern, as it has the potential to migrate toward the heat source (Stormont 1997; Beauheim and Roberts 2002; Hansen 2008). Additionally, the fracturing of salt caused by temperature changes and the resulting pore pressure changes, particularly in the presence of high-heat-emitting waste packages, can enhance the transport of gas and brine toward the heat source (Hansen and Leigh 2011). Such migration has the potential to compromise the integrity of nuclear waste disposal facilities, as brine can corrode metal waste containers and facilitate the transport of radionuclides if released.

To address these challenges and ensure the safe disposal of nuclear waste in salt repositories, it is crucial to quantitatively predict brine flow and its evolution with time and temperature under representative stress and pressure conditions.

Previous field tests conducted in the 1990s or earlier have characterized the movement of brine in rock salt under different temperature conditions (Ewing 1981; Krause 1983; McTigue and Nowak 1987; Coyle et al. 1987; Finley et al. 1992). These tests demonstrated that without heating, the brine inflow response varied due to the heterogeneity of the tested rock salt formations (Finley et al. 1992). When heating was applied, the experiments showed that brine inflow rates increased with increasing borehole temperature, and significant brine release occurred during heater shutdown (Ewing 1981; Coyle et al. 1987). However, previous efforts to simulate these experiments faced significant challenges in accurately predicting brine inflow. Uncoupled or loosely coupled models utilized in these attempts could only provide a qualitative approximation of certain aspects of the data, limiting their predictive capabilities. Other limitations stemmed from data quality issues caused by power fluctuations or brine leaks (Kuhlman and Malama 2013). Moreover,

the cooling phase was rarely properly planned for in the experiment or successfully reproduced by the modeling.

To address these gaps, the Brine Availability Test in Salt (BATS) is conducted at the Waste Isolation Pilot Plant (WIPP) in New Mexico by the US Department of Energy (Kuhlman et al. 2020; Guiltinan et al. 2020; Jayne and Kuhlman 2020; Kuhlman et al. 2021). The WIPP serves as the current US disposal facility for non-heat-emitting radioactive waste. The BATS experiment involves a series of horizontal-borehole tests conducted in the salt formation approximately 650 m below the surface with the objective of providing clean data for developing and testing the predictive capabilities of existing simulators and constitutive models for rock salt at a repository scale (Kuhlman 2020).

To accurately model the BATS experiment, a coupled thermo-hydro-mechanical (THM) modeling framework is imperative, as it accounts for the complex interactions between thermal effects, brine migration, and mechanical behavior, specifically addressing the creep, and damage phenomena exhibited by salt.

Building upon our previous work, where we successfully modeled a laboratory borehole heating/cooling experiment under zero initial stress and atmospheric pressure conditions (Tounsi et al. 2023), we extend our modeling efforts to the BATS 1a experiment to investigate the challenges and complexities associated with brine migration under more realistic conditions. The insights gained from this study will contribute to a better understanding of the behavior of brine in salt repositories and improve the overall safety and effectiveness of long-term nuclear waste disposal.

The remainder of this paper is organized as follows. In Sect. 2, the BATS experiment is briefly described. In Sect. 3, we provide an overview of the TOUGH–FLAC environment and the mechanical, thermal, and hydraulic constitutive models used to characterize the behavior of rock salt in the simulations. In Sect. 4, we present the results of the THM coupled modeling, including the analysis of temperature evolution, water flow rate, and damage in light of the measurements from the BATS 1a experiment. Finally, the implications of the experimental and numerical modeling findings from the BATS experiment on repository-scale operations are discussed in Sect. 5.

2 The BATS 1a Experiment

This research paper focuses on BATS phase 1a, which refers to testing that occurred from January to March 2020. It comprised two identical horizontal-borehole arrays drilled in the wall of a drift at WIPP within the clean halite geological unit: one subjected to heating and the other serving as a control, as shown in Fig. 1.

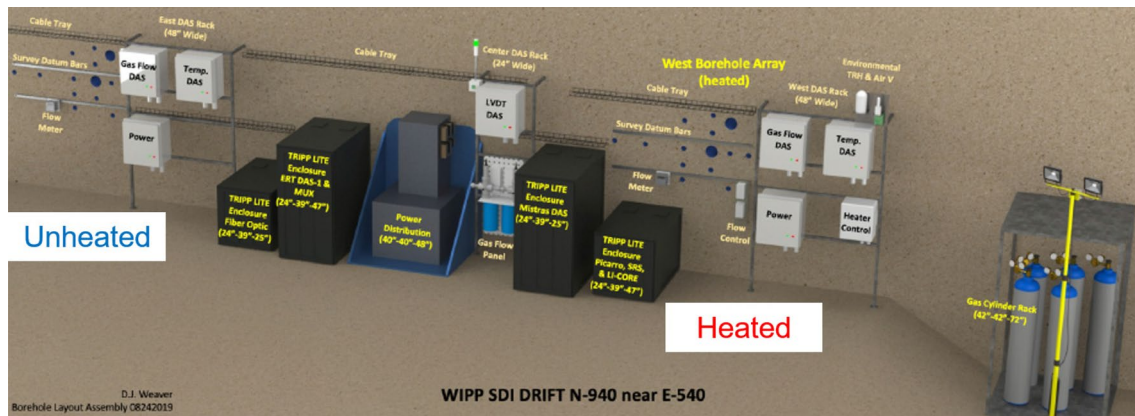


Fig. 1 View of the drift wall showing the layout of boreholes and test equipment (Kuhlman et al. 2021)

Both arrays operate in parallel and are equipped with similar instrumentation, including sensors in the central borehole and surrounding boreholes, enabling comparative analysis. The central borehole is equipped with an inflatable packer to isolate moisture, which is removed by flowing dry nitrogen, as can be seen in Fig. 2a. Gas mass flow rate is measured at 15-min intervals, and the cumulative mass of water leaving the system is derived from these observations. To validate the measurements, the output gas is periodically weighed after passing through a desiccant. In the heated array, a 750-watt heater is installed in the central borehole, enabling heating of a 60-centimeter interval. The duration of the heating phase is approximately one month, followed by a cooling phase.

The surrounding boreholes in the array, shown in Fig. 2b, are instrumented to measure temperature distribution and strain using thermocouples and fiber optics distributed sensing. Acoustic emissions, indicative of rock salt damage from heating and cooling, are monitored, and electrical resistivity tomography is employed in select boreholes. More details on the instrumentation of the BATS 1a experiment can be found in Kuhlman et al. (2020), Kuhlman et al. (2021).

The measurements obtained from the BATS experiment, as reported in Kuhlman et al. (2020), Kuhlman et al. (2021), reveal jumps in water flow rate in the heated array during transitions in heater power, with the highest flow jump occurring during cooling. In contrast, the unheated array shows relatively constant water flow rate. Acoustic emission activity also demonstrates distinct patterns between the heated and unheated arrays. There are pronounced increases in response to changes in heater power, and turning off the heater leads to acoustic emission activity more than five times higher than that observed during the initial heating phase. In contrast, the unheated array exhibits more consistent acoustic emission activity.

3 Numerical Methods

3.1 TOUGH–FLAC Simulator

In this study, a macroscopic formulation was employed to investigate the non-isothermal two-phase flow through deformable porous media, specifically rock salt. The model incorporated phenomenological models, including creep, shear and tensile-induced dilatancy/damage and healing to accurately capture the influence of these factors on the flow properties of the rock salt.

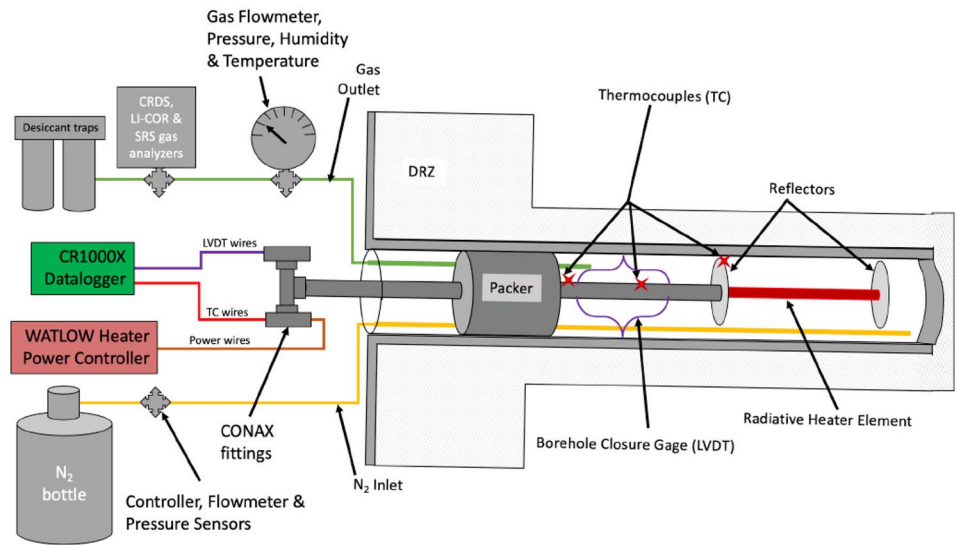
The TOUGH–FLAC simulator was utilized, which integrates the capabilities of TOUGH2, an integral finite difference simulator for multiphase flow and heat transport, and FLAC^{3D}, a finite difference geomechanical code (Pruess et al. 2012; Itasca FLAC3D 2012). To solve coupled problems, TOUGH–FLAC adopts the fixed-stress sequential method, whereby the energy and mass transfer phenomena are initially solved under a constant total stress field (Kim et al. 2011). Subsequently, the geomechanical problem is addressed using the updated fluid phase pressures, saturations, and temperature fields (Rutqvist et al. 2002).

The thermodynamic state of the liquid and gas phases is determined using the EOS4/TOUGH module, which accounts for the vapor pressure reduction resulting from capillary pressure effects (Pruess et al. 2012).

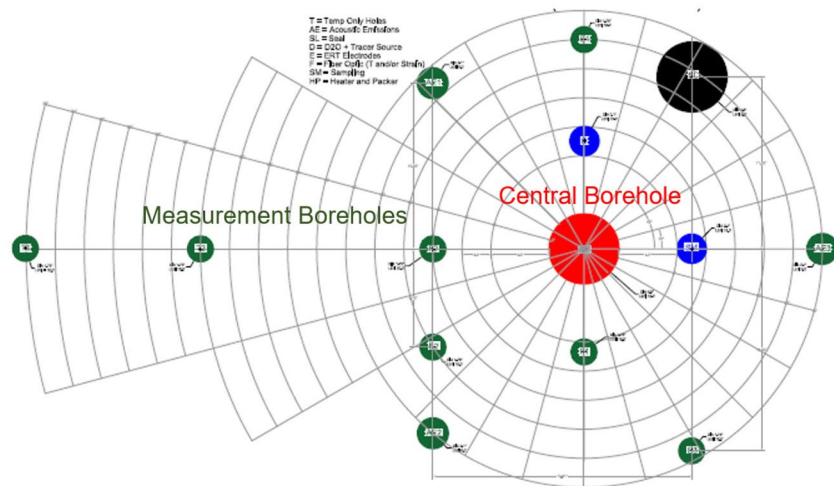
To account for large deformations of the solid material, TOUGH–FLAC was extended by employing an updated Lagrangian approach, which involved updating the computational grid at each time step (Blanco-Martín et al. 2017). Additionally, the mechanical simulation enables the adjustment of flow properties, namely permeability, porosity, and capillary pressure, based on the computed stress and strain fields.

The stress–strain constitutive relationship was expressed in terms of effective stress, with the total strain

Fig. 2 Configuration of the central heated borehole and locations of the measurement boreholes (Kuhlman et al. 2020)



(a) Schematic view of the central heated borehole.



(b) Location of measurement boreholes

tensor ϵ partitioned into elastic ϵ^e , viscoplastic ϵ^{vp} , and thermal ϵ^{th} components, as follows:

$$\dot{\sigma}' = \dot{\sigma} + B\dot{\omega}\mathbf{1} = \mathbf{H} : (\dot{\epsilon} - \dot{\epsilon}^{vp} - A_T \dot{T}\mathbf{1}), \quad (1)$$

where σ and σ' are, respectively, the total and effective stress tensors (negative values denote compressive stresses), A_T is the drained linear thermal expansion coefficient, B is the Biot coefficient, \mathbf{H} is the drained elasticity tensor and ω is the equivalent pore pressure. The latter is defined as the sum of the saturation weighted sum of the pressures of the liquid (λ) and gas phases (γ) and an interfacial energy term (Coussy 2004):

$$\omega = (1 - S_\lambda)p_\gamma + S_\lambda p_\lambda + \int_{S_\lambda}^1 p_c(S)dS \quad (2)$$

with $p_c = p_\gamma - p_\lambda$ the capillary pressure.

The balance equations solved in TOUGH and FLAC, together with Darcy's law for the filtration velocity vector of fluid phases, Fourier's law for the conductive heat flux, and Fick's law for the diffusive velocity vector of water vapor, must be supplemented by constitutive equations of rock salt.

The evolution of porosity is governed by changes in temperature and pressures of the liquid and gaseous phases via empirical coefficients that depend on the thermal expansion coefficient, the porosity, the Biot coefficient and the drained bulk modulus K .

$$d\phi = C_p(B, K, \phi) \sum_{\alpha} S_{\alpha} dp_{\alpha} + C_T(A_T, \phi) dT + \Delta\phi. \tag{3}$$

The term $\Delta\phi$ is a porosity correction that was introduced to account for volume changes resulting from the geomechanical calculations in FLAC^{3D}, in the resolution of the mass and energy balance equations in the next time step. For a detailed derivation of this term as a function of temperature, phase pressures, and total volumetric strain, further details can be found in the work by Kim et al. (2012).

3.2 Constitutive Equations of Rock Salt

3.2.1 Mechanical Constitutive Model

The Lux/Wolters (LW) model (Wolters et al. 2012; Blanco-Martín et al. 2016) is used in this study to characterize the mechanical behavior of rock salt.

The viscoplastic strain rate tensor, denoted as $\dot{\epsilon}^{vp}$, in the LW model is decomposed into three components: the viscous shear strain rate $\dot{\epsilon}^{vs}$, the damage-induced strain rate $\dot{\epsilon}^d$ resulting from shear or tensile failure, and the healing-induced strain rate $\dot{\epsilon}^h$:

$$\dot{\epsilon}^{vp} = \dot{\epsilon}^{vs} + \dot{\epsilon}^d + \dot{\epsilon}^h. \tag{4}$$

The viscous component is based on the modLubby2 constitutive model (Lerche 2012), which solely accounts for deviatoric effects and considers both transient and steady-state creep mechanisms. The expression of the damage strain rate component $\dot{\epsilon}^d$ and the dependence of elastic parameters on damage can be found in Lux et al. (2018). The healing component $\dot{\epsilon}^h$ is detailed in works by Lerche (2012) and Wolters (2014). A total of 40 parameters, obtained from the laboratory database of Clausthal University of Technology (Lerche 2012; Lux et al. 2018), were used to describe all deformation stages: elasticity, transient and stationary creep, shear and tensile damage and healing.

3.2.2 Hydraulic and Thermal Constitutive Models

Thermomechanically induced damage in rock salt results in the development of micro-fissures, which can lead to the generation of a secondary permeability when viscoplastic volumetric strain ϵ_v^{vp} exceeds a dilatancy threshold $\epsilon_{v,0}^{vp}$ and the coalescence of damage-induced micro-fissures occurs (Wolters et al. 2012). The permeability–dilatancy relationship is expressed as follows:

$$\begin{cases} \log(k) = \log(k_0) + \left\langle \log(\epsilon_v^{vp}) - \log(\epsilon_{v,0}^{vp}) \right. \\ \quad \left. + \frac{r}{\ln(10)} \exp(s\sigma'_{12}) \left(\text{Ei}(t\epsilon_v^{vp}) - \text{Ei}(t\epsilon_{v,0}^{vp}) \right) \right\rangle; \\ \epsilon_v^{vp} \geq \epsilon_{v,0}^{vp} \\ k = k_0; \epsilon_v^{vp} < \epsilon_{v,0}^{vp} \end{cases}, \tag{5}$$

where k_0 represents the initial/minimum permeability of rock salt, σ'_{12} denotes the effective stress perpendicular to the micro-fissure orientation, $\text{Ei}(x)$ stands for the exponential integral function, and r , s , and t are material constants.

Furthermore, hydraulically induced damage can result in an increase in intrinsic permeability when the equivalent pore pressure ϖ exceeds the minimum (i.e., least compressive) principal stress σ_3 , leading to the opening of grain boundaries and fluid infiltration Wolters et al. (2012). This relationship is expressed as:

$$\log(k) = i_1 + i_2 \arctan(i_3 \Delta P_{fl}) + i_4 \exp(i_5 \Delta P_{fl}), \quad \Delta P_{fl} > 0, \tag{6}$$

where $\Delta P_{fl} = \varpi + \sigma_3$ and i_1, i_2, i_3, i_4 and i_5 are material parameters.

The Biot coefficient of undisturbed rock salt, initially very low, is assumed to increase with the level of damage using the following analytical formula (Hou 2002; Kansy 2007):

$$B = \max\left(\frac{D}{0.1}, 1 - \exp\left(\frac{\sigma_{vM} m D}{D - 0.1}\right)\right), \tag{7}$$

where D represents the damage variable, ranging between 0 and 1, and m is the LW model parameter controlling the influence of the equivalent stress on the Maxwell viscosity coefficient. When the shear stress exceeds the dilatancy boundary, the time derivative of D is proportional to the sum of the shear and tensile yield functions. If the stress state falls below the sealing/healing boundary, the time derivative of D is expressed as a function of the healing boundary. Furthermore, if rock salt has fully healed, the initial values of the intrinsic permeability and Biot’s coefficient will be restored.

Changes in permeability and porosity influence the magnitude of capillary pressure. To account for this, the capillary pressure is scaled using the following formula (Leverett 1941):

$$p_c = p_{c_0} \left(\frac{k_0/\phi_0}{k/\phi} \right)^l \tag{8}$$

p_{c_0} denotes the unscaled capillary pressure, expressed using the van Genuchten model:

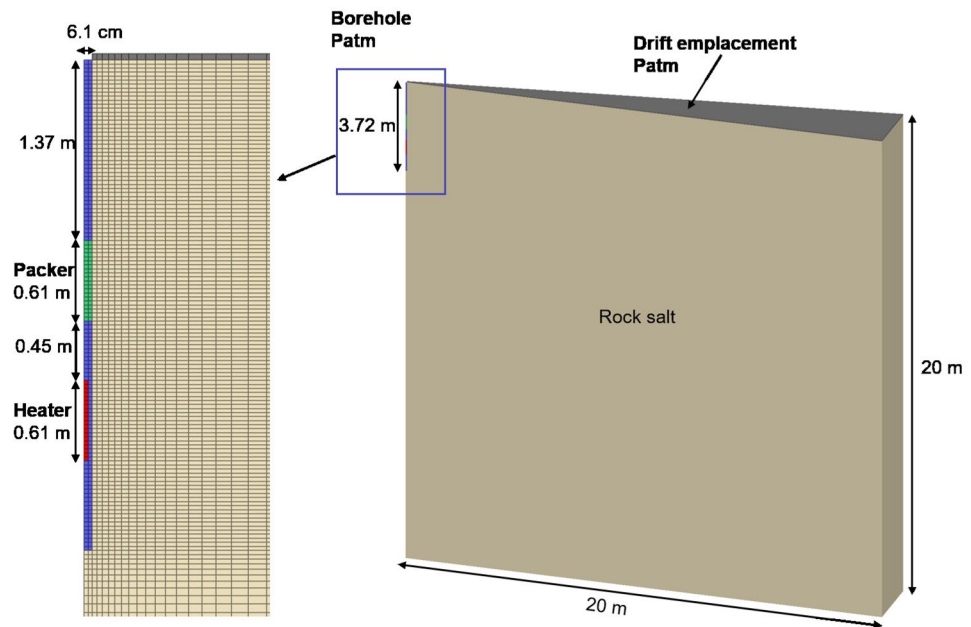
$$p_{c_0} = -P_0 \left([S^*]^{-1/\mu} - 1 \right)^{1-\mu}; \quad p_{c_0} \geq P_{\max}, \tag{9}$$

where $S^* = (S_{\lambda} - S_{\lambda r}) / (1 - S_{\lambda r})$. Parameters $P_0, \mu, S_{\lambda r}, P_{\max}$ and l are material constants and ϕ_0 represents the initial porosity of the porous medium.

Corey’s curves are used to express liquid and gas relative permeabilities.

Regarding the thermal parameters, the evolution of thermal conductivity and heat capacity of rock salt with

Fig. 3 Geometry used for the THM simulation of brine inflow into a heated borehole in the BATS experiment



temperature is described using the following empirical expressions derived within the BAMBUS project (Bechthold et al. 2004):

$$\begin{cases} C_p = 855 + 0.1777 T \\ \lambda_{\text{salt}} = 5.734 - 1.838 \times 10^{-2} T + 2.86 \times 10^{-5} T^2 \\ \quad - 1.51 \times 10^{-8} T^3 \end{cases} \quad (10)$$

4 Numerical Modeling of the BATS 1a Experiment

4.1 Model Setup: Geometry, Boundary and Initial Conditions, and Simulation Phases

The model geometry used in this study is a 9° cylindrical sector with an outer radius of 20 m and a height of 20 m, as illustrated in Fig. 3. A borehole measuring 3.73 m in length and 0.061 m in radius is excavated from the top center of the cylinder; it is equipped with a heater and an impermeable packer. Only the TOUGH mesh contains the borehole grid elements, including the heater and the packer elements. The dimensions of the cylindrical sector were chosen to ensure that the temperature, pore pressure, and stress near the bottom and the right boundary are undisturbed by changes around the borehole.

Boundary and initial conditions play a crucial role in simulating the THM system accurately. An atmospheric pressure boundary condition with a humidity level of 70% is applied to the top boundary, to represent the drift, and to

the borehole grid elements. All other boundaries are set to no-flow. The right boundary maintains a constant normal stress of -14 MPa and all the other boundaries are set to no-displacement normal to the boundary surfaces. Finally, the heat flux at all boundaries is zero.

Initially, the system is set to total stress, pore pressure, liquid saturation, and temperature of -14 MPa, 8 MPa (value comprised between the hydrostatic and lithostatic stress), 1, and 28°C , respectively, with the gravitational variation of stress and pore pressure neglected. It should be noted that the excavation of the drift is not simulated, and it is assumed that the near-drift damaged zone has fully healed when the borehole was excavated, maintaining the stress at -14 MPa.

4.2 Material Parameters and Simulation Phases

Table 1 lists the THM properties of rock salt. Many of these values come from prior research on natural salt (Bechthold et al. 2004; Blanco-Martín et al. 2016). Parameters of Eqs. 5 and 6 can be found in Wolters (2014) and, hence, are not provided here.

The initial permeability of rock salt is representative of the permeability at WIPP.

The simulation starts with the excavation of the borehole, after which the stress and pore pressure are allowed to redistribute for a period of 300 days. Figure 4 shows the distribution of pore pressure and permeability around the borehole, after 300 days. It is observed that the gradient of pore pressure around the borehole is now governed by a rock salt pressure that is significantly lower than the initial pressure of 8 MPa. Furthermore, the permeability which was initially equal to $5 \times 10^{-22} \text{ m}^2$ has become equal to

Table 1 Parameters of rock salt used in the numerical simulations

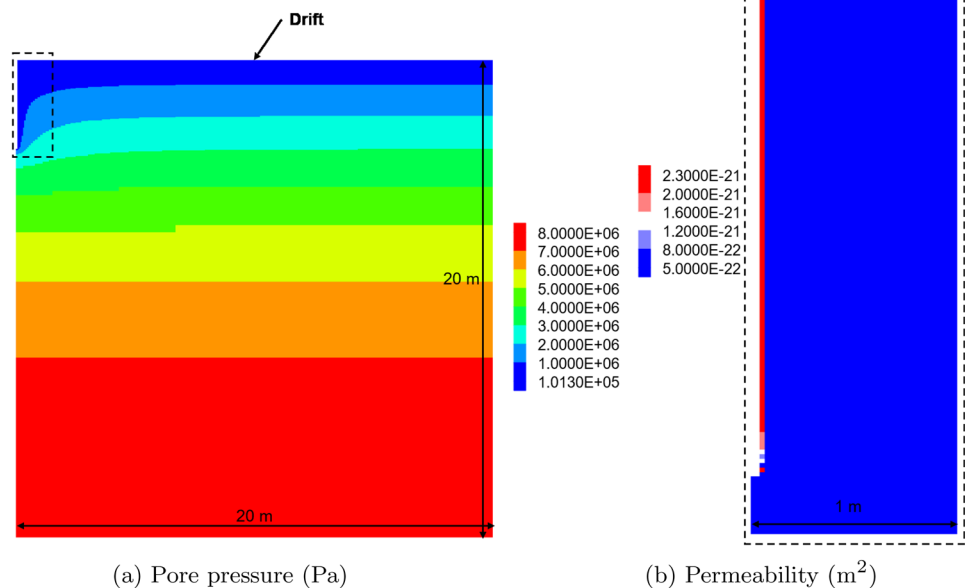
Property (unit)	Value
Solid density ρ_σ (kg/m ³)	2154
Initial porosity ϕ_0	0.001
Initial permeability k_0 (m ²)	5×10^{-22}
Dilatancy limit $\varepsilon_{v,0}$	9×10^{-4}
Initial Biot coefficient	0.0015
Initial drained bulk modulus K_{dr} (GPa)	20
Linear thermal expansion coefficient A_T (K ⁻¹)	40×10^{-6}
Corey's residual liquid saturation S_{lr}	0.05
Corey's residual gas saturation S_{gr}	0
van Genuchten's μ	0.6
van Genuchten's P_0 (MPa)	5.7
van Genuchten's S_{lr}	0.01
Parameter l of Eq. 8	0.57

2.3×10^{-21} m² (roughly 5 times higher) over a radius equal to half the borehole's radius. Indeed, excavation-induced shear stresses lead to shear dilatancy in the Excavation-Damaged Zone (EDZ) around the borehole, which results in an increase in permeability.

Following this phase, a heating phase lasting a month is conducted, followed by a shutdown phase. Figure 5 shows the heat power function applied to the heater. Note that from here onwards, $t = 0$ will refer to post 300 days.

4.3 Results and Discussion

In this section, we present and interpret the results of our simulations in comparison to the measurements of

Fig. 4 Distribution of pore pressure and permeability at the end of the open-borehole phase


temperature, brine inflow rate, cumulative brine inflow, and acoustic emissions activity in the BATS experiment, phase 1a.

4.3.1 Evolution of Temperature

The evolution of temperature plays a critical role in the behavior of the rock salt during the BATS experiments, as it is a driving force behind various hydraulic and mechanical changes. The accuracy of the temperature evolution predicted by our model was validated by comparing it with temperature measurements at five monitoring points, as shown in Figs. 6 and 7 (the colors of the curves in Fig. 6 correspond to the colors representing the locations of the thermocouples in Fig. 7). The simulation results agreed well with the measured temperature evolution in all of the monitoring points. It should be noted that accounting for the temperature dependency of thermal conductivity was necessary to accurately reproduce temperature measurements (see Eq. 10).

Moreover, as observed in the temperature contour maps, the temperature distribution was initially symmetrical during heating but became asymmetric after 25 days due to the presence of the drift. Therefore, it is important to consider a model that goes beyond a one-dimensional representation to accurately predict temperature distribution and associated mechanical and hydraulic changes throughout the rock salt mass.

4.3.2 Evolution of Brine Inflow into the Borehole

Figure 8 shows the simulated and measured brine inflow rate and cumulative inflow. Results of the unheated case are also

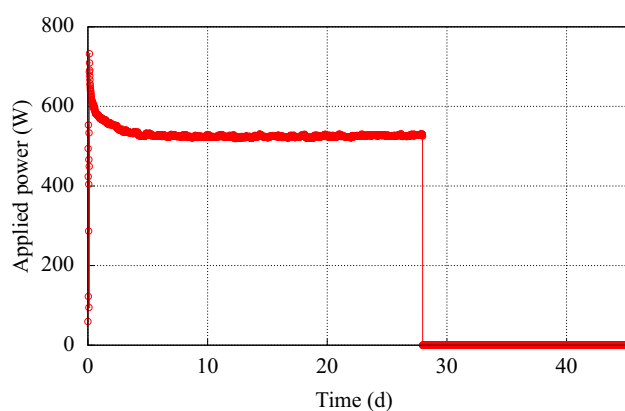


Fig. 5 Heater power evolution with time

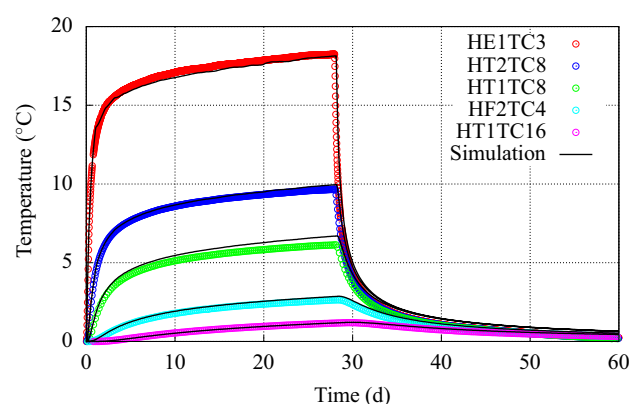


Fig. 6 Comparison of measured and simulated temperature in different locations

presented for comparison purposes. The inflow rate simulation results cover the entire duration of the simulation for the heated array, including the initial 300 days for which no inflow measurements were available.

During the heating phase, the brine inflow rate exhibited a peak that closely aligned with our model predictions. Notably, this alignment improved after incorporating the 300-day open-borehole phase, which prevented an overestimation of the predicted brine inflow rate peak. Moreover, our model accurately predicts the peak of the brine inflow rate when the heater is shut down.

However, upon closer examination of the zoomed-in figure, discrepancies between the modeling results and field measurements become apparent. Specifically, there was a distinct change in the dry gas flow rate behind the packer in the central boreholes of the heated and unheated arrays at around 6 days, which explains the flow rate change in the unheated array (Fig. 8b). This change likely affected the accuracy of brine inflow measurements during the initial

period in the heated array, contributing to the observed discrepancies.

Additionally, while the observed inflow rate stabilizes at the peak for a period of time before decreasing and then increasing again at 32 days when the heater is shut down, our simulation depicts an immediate decrease in the brine inflow rate following the peak. Addressing this discrepancy may involve adjusting the empirical evolution of the hydro-mechanical coupling properties used in the model, such as the permeability and the Biot coefficient. These properties were initially calibrated using a different salt material under specific stress, pore pressure, and temperature conditions.

In the next two paragraphs, the factors contributing to brine inflow during each stage will be analyzed.

4.3.3 Evolution of Pressure

Figure 9 shows the pressure profiles within a 6 m radius around the borehole at mid-depth of the heater on different dates. Pressure here designates the maximum of the gas phase pressure and the liquid phase pressure. The blue curve represents the initial pressure prior to the heating phase. One day after activating the heater, the green curve demonstrates an increase in pore pressure, reaching just below 3.5 MPa. This rise in pore pressure can be attributed to thermal pressurization of the pore fluid, which is the primary mechanism controlling the increase in inflow when the heater is turned on. When the heater is turned off, the pore pressure has nearly returned to its initial pre-heating state. As the rock salt cools down, the pore pressure drops below atmospheric pressure around the borehole, signifying a gradual desaturation of the rock.

4.3.4 Evolution of Stress, Dilatancy, and Permeability

The analysis of the total stress evolution in four locations (P1, P2, P3, P4) at mid-depth of the heater and within a 1 m radius from the borehole uncovers noteworthy patterns (see Fig. 10a). During the heating phase, the minimum principal stress exhibits negative values, indicating a compressive stress state. Notably, stress peaks occur when the heater is turned on due to the thermal expansion of rock salt. When the cooling phase starts, the stress state transitions to a tensile state in the two locations situated within 16 cm from the borehole wall (P1 and P2), resulting in tensile failure of the rock salt.

Figure 10b and c show the simulated evolution of dilatancy and permeability ratio. The permeability ratio is defined as the current permeability divided by the initial permeability of undisturbed salt. These dilatancy and permeability changes occur in response to stress variations in the

Fig. 7 Temperature ($^{\circ}\text{C}$) contour maps at two dates. Locations of the temperature sensors are given (coordinates unit in meters)

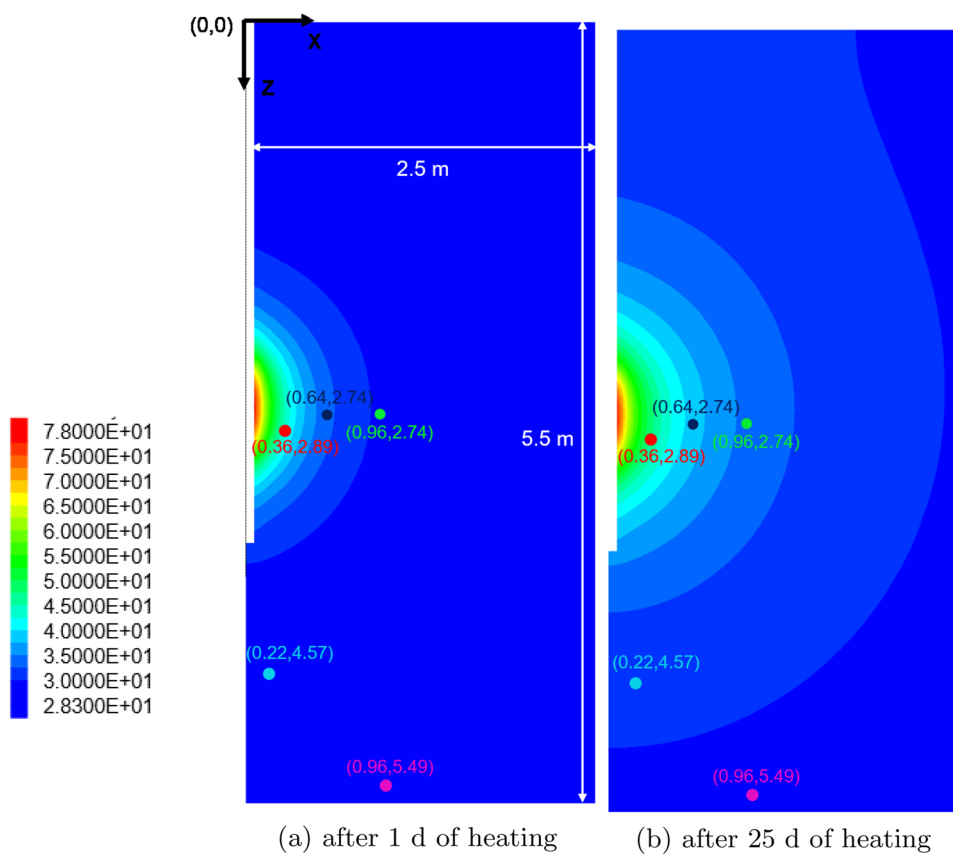
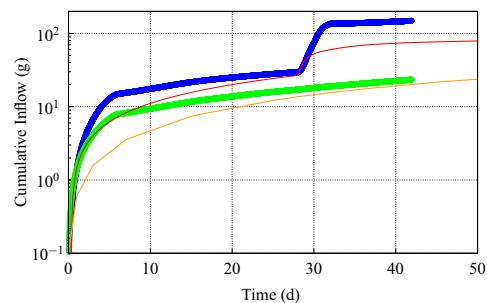
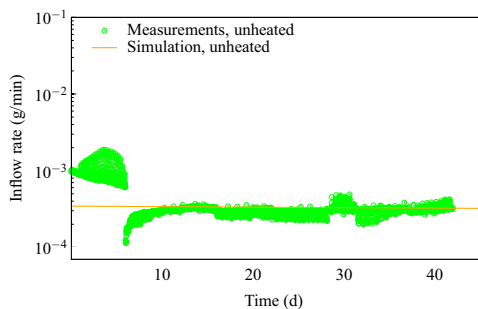
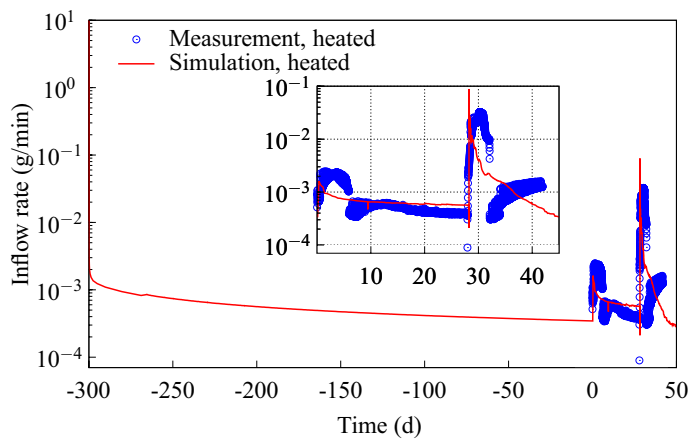


Fig. 8 Comparison of simulated and measured brine inflow rate and cumulative brine inflow in the heated and unheated arrays



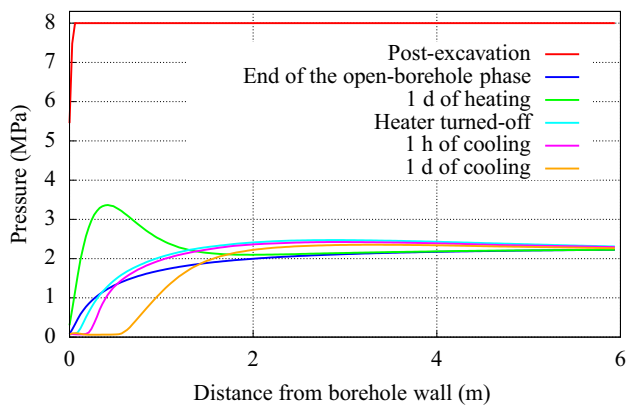


Fig. 9 Liquid/gas pressure profile at mid-depth of the heater (-2.73 m) at different dates

two locations closest to the borehole wall (P1 and P2), which are highly susceptible to temperature and stress fluctuations.

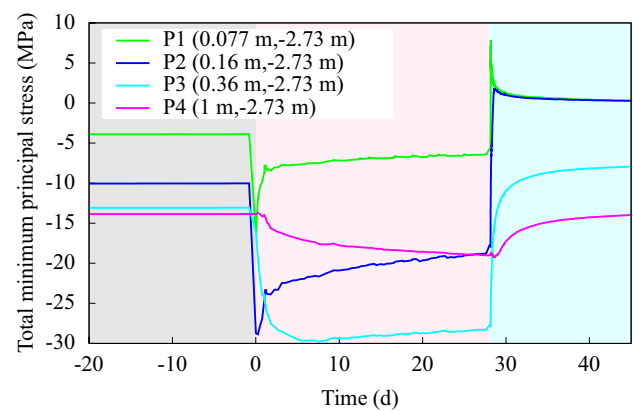
Prior to heating, dilatancy, and permeability changes in location P1 can be attributed to the excavation-induced shear stresses, leading to shear dilatancy and subsequent permeability increase. The simulations predict that the EDZ of the borehole extends to a radius approximately equal to half the borehole radius, with a permeability roughly five times higher than the initial permeability (Fig. 4).

Upon activation of the heater, a decrease in dilatancy is observed, indicating the occurrence of healing processes within the EDZ. Consequently, permeability instantaneously decreases. However, as stress relaxation occurs, rock salt undergoes dilation once again, driven by both heating-induced shear stresses and excavation-induced shear stresses. As a result, permeability increases, predominantly near the borehole wall where compressive stresses are relatively lower in magnitude.

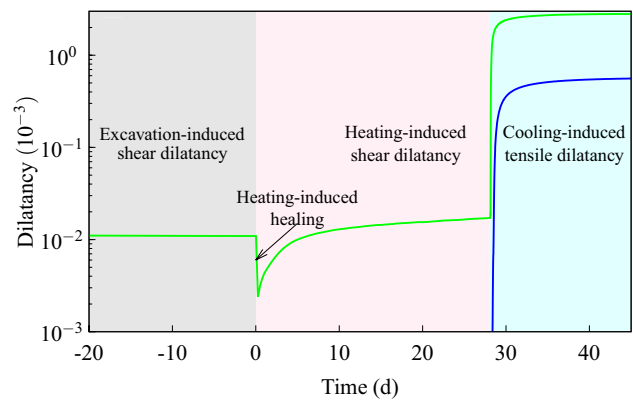
During the cooling phase, dilatancy induced by tensile stresses is predicted. This phenomenon exhibits the highest magnitude and leads to a substantial four-order-of-magnitude increase in permeability.

The extent of cooling-induced damage is illustrated in Fig. 11. The damaged zone symmetrically develops around the heater, with a maximum width of 22 cm, equivalent to three and a half times the heater's radius, and a length of 1.23 m, approximately twice the length of the heater.

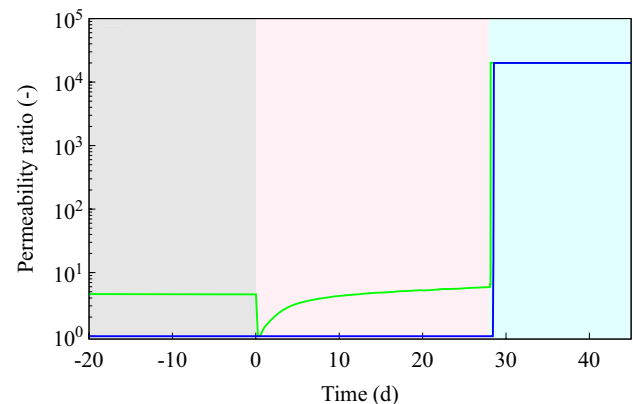
To experimentally validate the simulated magnitude of thermo-mechanical damage, a comparison was conducted between the evolution of the damage variable D and the total number of acoustic emissions (AE) hits measured during the BATS experiment. To achieve this, the maximum value standardization method was utilized to scale the compared values between 0 and 1, with the maximum value of damage/acoustic emissions hits set as 1. Figure 12 presents the two standardized curves. A strong positive correlation



(a) Minimum stress



(b) Dilatancy



(c) Permeability

Fig. 10 Evolution of the minimum stress, dilatancy and permeability in different locations at mid-depth of the heater

is observed between the damage variable and the acoustic emissions activity. However, the increase in damage during the heating phase is more gradual and of lesser magnitude compared to the acoustic emissions activity. Both curves indicate that turning off the heater leads to a greater damage/acoustic emissions activity than the initial heating phase, although the model overestimates this increase: the acoustic

Fig. 11 Evolution of permeability (m^2) during cooling

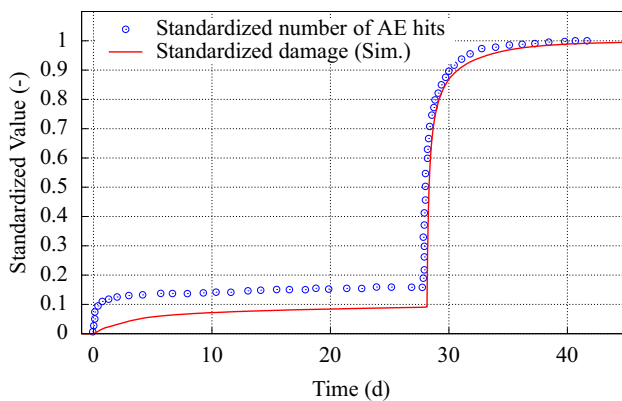
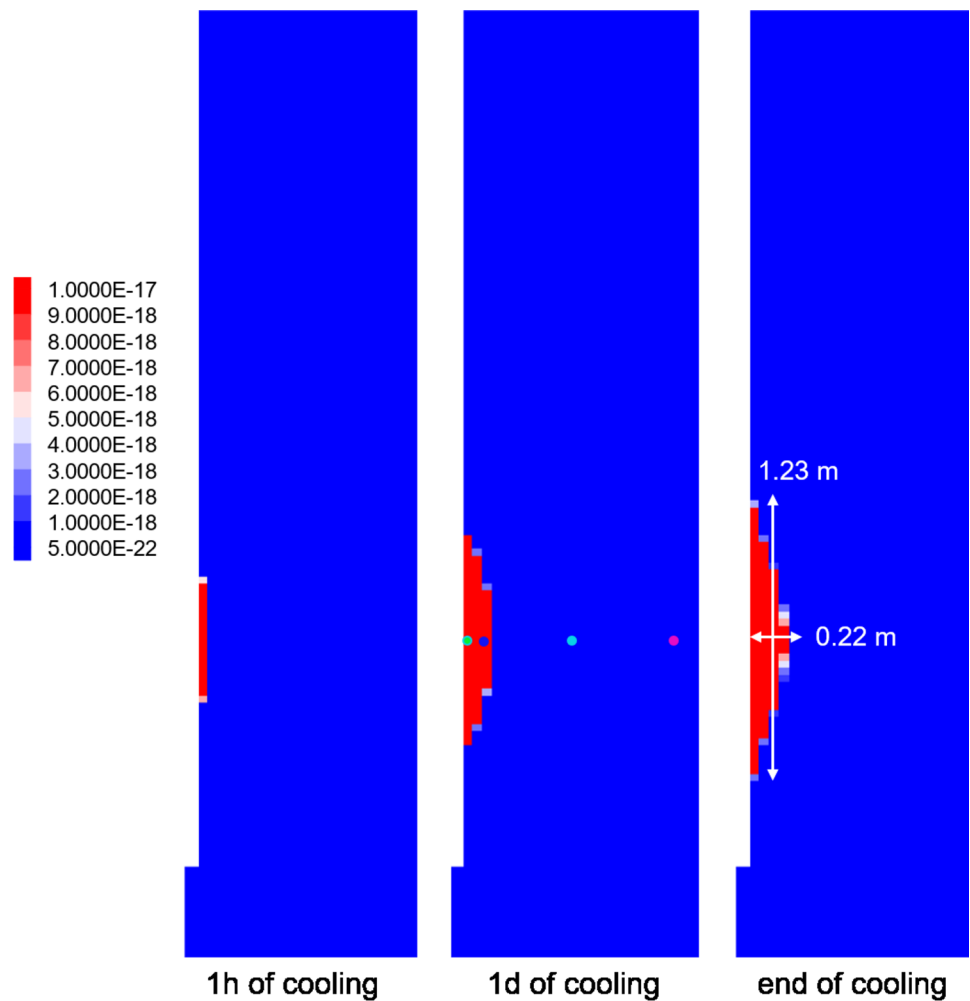


Fig. 12 Correlation between simulated damage and the measured total number of acoustic emissions hits

emissions activity is 6.7 times larger compared to a tenfold increase in damage.

4.3.5 Effect of the Biot Coefficient

In this section, we compare the results of the previously presented simulation, which utilized a low Biot coefficient that increases with damage, reaching 10 times its initial value after the cooling phase, with a new simulation incorporating a Biot coefficient that is constant and 100 times higher, similar to the value used by *McTigue (1986)*. The focus is on examining the brine inflow rate and pore pressure profiles during the heating and cooling phases, as shown in *Figs. 13 and 14*.

Significant differences emerge between the two simulations. With the higher Biot coefficient, the thermal pressurization effect is considerably stronger, resulting in a pore pressure of 20 MPa during the heating phase. This exceeds the minimum principal stress, resulting in hydraulic damage to the rock salt surrounding the borehole and an increase in its permeability. Consequently, the simulation predicts a higher inflow rate peak when the heater is turned on and a slower decline due to the presence of elevated pressure gradients.

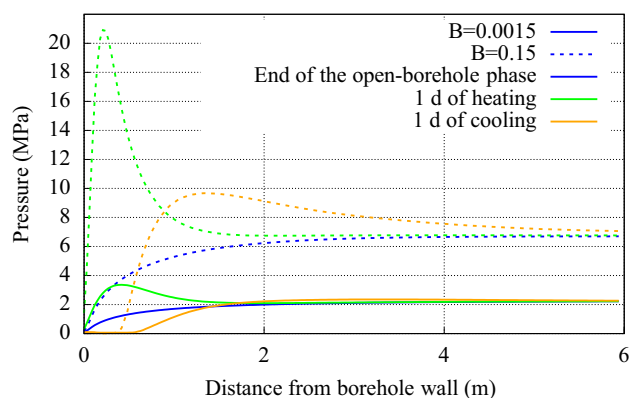


Fig. 13 Effect of the Biot coefficient on the pressure profiles

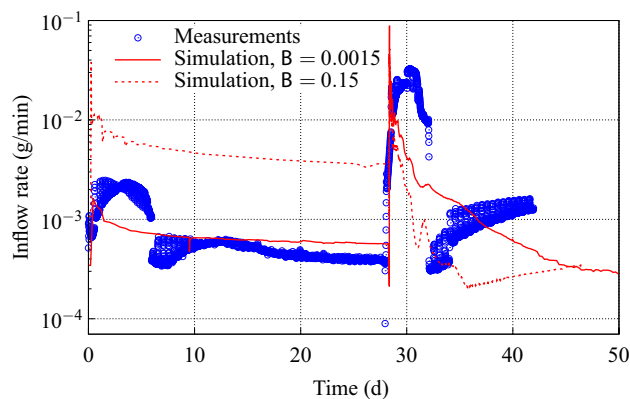


Fig. 14 Effect of the Biot coefficient on the brine inflow rate

A notable observation arises from the comparison of the brine inflow rate after the cooling peak. The dashed curve, representing the simulation with the higher Biot coefficient, demonstrates a closer adherence to the shape of the measured curve, particularly in capturing the post-peak increase in inflow rate. This finding suggests that while an initial low Biot coefficient may provide accurate results, it appears that the subsequent increase of the Biot coefficient with thermo-mechanical damage in our model is lower than what the measurements suggest.

5 Implications for Repository-Scale Operations

The BATS test and its numerical modeling provide valuable insights into how rock salt behavior can be influenced by varying thermal and mechanical conditions, carrying several crucial implications for salt repositories:

1. **Excavation-Damaged Zone (EDZ):** The EDZ plays a critical role in repository-scale operations. While smaller boreholes may result in a relatively modest EDZ, larger drift excavations generate higher shear stresses, leading to a more extensive EDZ. This expansion can significantly affect porosity and permeability in the surrounding geological formation (Stormont et al. 1992).
2. **Heating Effects:** Understanding the effects of heating is essential for repository-scale operations, especially given the extended duration of the heating period. Elevated temperatures during heating can have both positive and negative consequences. On one hand, heating can accelerate the closure of excavation-induced dilation in salt, reducing deviatoric stresses and permeability. However, it can also induce shear dilatancy and damage in areas where deviatoric stresses increase as a result of heating (Tounsi et al. 2023). Additionally, thermal expansion of the rock decreases its porosity and thermal expansion of the pore fluid leads to thermal pressurization, resulting in increased fluid inflow into the excavation. If the EDZ has not fully healed when the temperature starts to increase, its lower liquid saturation and high permeability may limit thermal pressurization and liquid relative permeability near the excavation, potentially reducing brine inflow. These effects, particularly in low-permeability geological formations found in repositories, must be addressed in design to ensure waste containment and overall safety.
3. **Cooling Effects:** During the cooling process, microfractures form within rock salt due to tensile failure induced by the contraction of the salt grains. This process leads to a rapid and notable increase in salt permeability in the proximity of the borehole, subsequently resulting in a surge of brine flow directed toward the borehole. Imposing a sufficiently low cooling rate could mitigate this substantial release of brine associated with cooling. At the repository level, radioactive decay rates lead to very gradual decrease of temperature, suggesting that the cooling effects may be of lesser concern.
4. **Future Research and Testing:** Enhancing our understanding of these intricate phenomena and their implications for repository-scale operations demands comprehensive research and testing. Experiments should investigate variable cooling rates to either confirm or

question the significance of cooling effects on brine migration in salt repositories. Furthermore, a broader range of temperature levels should be explored, alongside assessments conducted across various geological units.

6 Conclusion

In summary, this paper presents a numerical modeling study of the BATS 1a experiment, focusing on the thermo-hydro-mechanical behavior of rock salt surrounding a heated borehole. The model successfully replicates key aspects of the experiment, including temperature distribution, brine inflow rate, cumulative inflow, and damage evolution, by incorporating relevant geometry, boundary and initial conditions, and constitutive equations.

The use of a 2D axisymmetric model and temperature-dependent thermal conductivity improves the simulation's accuracy, enabling the representation of temperature distribution asymmetry and validation against measured data. The analysis of brine inflow demonstrates good agreement during the heating and shutdown phases. However, further calibration and a better understanding of flow characteristics and their evolution with damage are necessary to address discrepancies between simulated and measured inflow rate and damage. Analysis of pressure and stress shows that thermal pressurization and tensile-induced damage of rock salt are the primary contributors to observed brine inflow spikes during heating and cooling.

These insights into the THM behavior of rock salt have important implications for understanding brine flow in deep geological repositories. Future directions could involve incorporating additional experimental data, refining the model through further calibration, and analyzing new BATS phases that involve multistage variations in heater power and address the gas flow rate issues at the start of the heating stage. This continued research will contribute to a more comprehensive understanding of rock salt behavior and enhance the predictive capabilities of THM models in various geotechnical applications, including nuclear waste disposal.

Acknowledgements DECOVALEX is an international research project comprising participants from industry, government and academia, focusing on development of understanding, models and codes in complex coupled problems in sub-surface geological and engineering applications; DECOVALEX-2023 is the current phase of the project. The authors appreciate and thank the DECOVALEX-2023 Funding Organizations Andra, BASE, BGE, BGR, CAS, CNSC, COVRA, US DOE, ENRESA, ENSI, JAEA, KAERI, NWMO, NWS, SÚRAO, SSM, and Taipower for their financial and technical support of the work described in this paper. The statements made in the paper are, however, solely those of the authors and do not necessarily reflect those of the Funding Organizations. This paper describes objective technical

results and analysis. Any subjective views or opinions that might be expressed in the paper do not necessarily represent the views of the U.S. Department of Energy or the United States Government. Sandia National Laboratories is a multi-mission laboratory managed and operated by National Technology & Engineering Solutions of Sandia, LLC (NTESS), a wholly owned subsidiary of Honeywell International Inc., for the U.S. Department of Energy's National Nuclear Security Administration (DOE/NNSA) under contract DE-NA0003525. This written work is authored by an employee of NTESS. The employee, not NTESS, owns the right, title and interest in and to the written work and is responsible for its contents. Any subjective views or opinions that might be expressed in the written work do not necessarily represent the views of the U.S. Government. The publisher acknowledges that the U.S. Government retains a non-exclusive, paid-up, irrevocable, world-wide license to publish or reproduce the published form of this written work or allow others to do so, for U.S. Government purposes. The DOE will provide public access to results of federally sponsored research in accordance with the DOE Public Access Plan.

Funding Funding for this work has been provided by the Spent Fuel and Waste Disposition Campaign, Office of Nuclear Energy of the U.S. Department of Energy, under Contract Number DE-AC02-05CH11231 with Lawrence Berkeley National Laboratory.

Data availability Data is already available online.

Declarations

Conflict of interest The authors have no competing interests to declare that are relevant to the content of this article.

Open Access This article is licensed under a Creative Commons Attribution 4.0 International License, which permits use, sharing, adaptation, distribution and reproduction in any medium or format, as long as you give appropriate credit to the original author(s) and the source, provide a link to the Creative Commons licence, and indicate if changes were made. The images or other third party material in this article are included in the article's Creative Commons licence, unless indicated otherwise in a credit line to the material. If material is not included in the article's Creative Commons licence and your intended use is not permitted by statutory regulation or exceeds the permitted use, you will need to obtain permission directly from the copyright holder. To view a copy of this licence, visit <http://creativecommons.org/licenses/by/4.0/>.

References

- Beauheim RL, Roberts RM (2002) Hydrology and hydraulic properties of a bedded evaporite formation. *J Hydrol* 259(1–4):66–88. [https://doi.org/10.1016/S0022-1694\(01\)00586-8](https://doi.org/10.1016/S0022-1694(01)00586-8)
- Bechthold W, Smailos E, Heusermann S, Bollingerfehr W, Bazargan Sabet B, Rothfuchs T, Kamlot P, Grupa J, Olivella S, Hansen FD (2004) Backfilling and sealing of underground repositories for radioactive waste in salt: Bambus II Project. Tech. Rep. EUR20621, European Atomic Energy Community
- Blanco-Martín L, Wolters R, Rutqvist J, Lux KH, Birkholzer JT (2016) Thermal-hydraulic-mechanical modeling of a large-scale heater test to investigate rock salt and crushed salt behavior under repository conditions for heat-generating nuclear waste. *Comput Geotech* 77:120–133. <https://doi.org/10.1016/j.compgeo.2016.04.008>
- Blanco-Martín L, Rutqvist J, Birkholzer JT (2017) Extension of TOUGH-FLAC to the finite strain framework. *Comput. Geosci.* 108:64–71. <https://doi.org/10.1016/j.cageo.2016.10.015>

- Chen J, Ren S, Yang C, Jiang D, Li L (2013) Self-healing characteristics of damaged rock salt under different healing conditions. *Materials* 6(8):3438–3450. <https://doi.org/10.3390/ma6083438>
- Cosenza P, Ghoreychi M, Bazargan-Sabet B, De Marsily G (1999) In situ rock salt permeability measurement for long term safety assessment of storage. *Int J Rock Mech Min Sci* 36(4):509–526. [https://doi.org/10.1016/S0148-9062\(99\)00017-0](https://doi.org/10.1016/S0148-9062(99)00017-0)
- Coussy O (2004) Poromechanics. John Wiley & Sons
- Coyle A, Eckert J, Kalia H (1987) Brine migration test report: asse salt mine, Federal Republic of Germany. Tech. Rep. BMI/ONWI-624, Office of Nuclear Waste Isolation, Columbus, OH (USA)
- Ewing RI (1981) Preliminary moisture release experiment in a potash mine in southeastern New Mexico. Tech. Rep. SAND-81-1318, Sandia National Laboratories, Albuquerque, NM (USA)
- Finley S, Hanson D, Parsons R (1992) Small-scale brine inflow experiments: Data report through June 6, 1991. Tech. Rep. SAND-91-1956, Sandia National Laboratories, Albuquerque, NM (USA)
- Guiltinan EJ, Kuhlman K, Rutqvist J, Hu M, Boukhalfa H, Mills M, Otto S, Weaver DJ, Dozier B, Stauffer PH (2020) Temperature response and brine availability to heated boreholes in bedded salt. *Vadose Zone J* 19(1):e20,019. <https://doi.org/10.1002/vzj2.20019>
- Hansen FD (2008) Disturbed rock zone geomechanics at the waste isolation pilot plant. *Int J Geomech* 8(1):30–38. [https://doi.org/10.1061/\(ASCE\)1532-3641\(2008\)8:1\(30\)](https://doi.org/10.1061/(ASCE)1532-3641(2008)8:1(30))
- Hansen FD, Leigh CD (2011) Salt disposal of heat-generating nuclear waste. Tech. Rep. SAND2011-0161, Sandia National Laboratories, Albuquerque, NM (USA), <https://doi.org/10.2172/1005078>
- Hou Z (2002) Geomechanische Planungskonzepte für untertägige Tragwerke mit besonderer Berücksichtigung von Gefügeschädigung, Verheilung und hydromechanischer Kopplung. Papierflieger, Clausthal-Zellerfeld, Germany
- Itasca FLAC3D (2012) 5.0 (Fast Lagrangian Analysis of Continua in 3 Dimensions) manual [55401]
- Jayne R, Kuhlman K (2020) Utilizing temperature and brine inflow measurements to constrain reservoir parameters during a salt heater test. *Minerals* 10(11):1025. <https://doi.org/10.3390/min10111025>
- Kansy A (2007) Einfluss des biot-parameters auf das hydraulische Verhalten von Steinsalz unter der Berücksichtigung des Porendruckes. PhD thesis, Technische Universität Clausthal, Clausthal-Zellerfeld, Germany
- Kim J, Tchelepi HA, Juanes R (2011) Stability and convergence of sequential methods for coupled flow and geomechanics: fixed-stress and fixed-strain splits. *Comput Methods Appl Mech Eng* 200(13–16):1591–1606. <https://doi.org/10.1016/j.cma.2010.12.022>
- Kim J, Sonnenthal EL, Rutqvist J (2012) Formulation and sequential numerical algorithms of coupled fluid/heat flow and geomechanics for multiple porosity materials. *Int J Numer Meth Eng* 92(5):425–456. <https://doi.org/10.1002/nme.4340>
- Krause WB (1983) Avery Island brine migration tests: Installation, operation, data collection, and analysis. Tech. Rep. ONWI-190 (4), Office of Nuclear Waste Isolation, Columbus, OH (USA)
- Kuhlman K (2020) DECOVALEX-2023 Task E Specification (Rev. 0). Tech. Rep. SAND-2020-4289R, Sandia National Lab.(SNL-NM), Albuquerque, NM (United States)
- Kuhlman K, Malama B (2013) Brine flow in heated geologic salt. Tech. Rep. SAND2013-1944, Sandia National Laboratories, Albuquerque, NM (USA), <https://doi.org/10.2172/1095129>
- Kuhlman K, Mills MM, Jayne R, Matteo EN, Herrick CG, Nemer M, Heath JE, Xiong Y, Choens RC, Stauffer P, Boukhalfa H, Guiltinan E, Rahn T, Weaver D, Dozier B, Otto S, Rutqvist J, Wu Y, Hu M, Uhlemann S (2020) FY20 Update on Brine availability test in salt. Tech. Rep. SAND-2020-9034R, M2SF-20SN010303032, Albuquerque, NM: Sandia National Laboratories
- Kuhlman K, Mills M, Jayne R, Matteo E, Herrick C, Nemer M, Xiong Y, Choens R, Paul M, Stauffer P, Boukhalfa H, Guiltinan E, Rahn T, Weaver D, Otto S, Davis J, Rutqvist J, Wu Y, Hu M, Uhlemann S, Wang J (2021) Brine Availability Test in Salt (BATS) FY21 Update. Tech. Rep. SAND2021-10962R, M2SF-21SN010303052, Albuquerque, NM: Sandia National Laboratories
- Lerche S (2012) Kriech- und Schädigungsprozesse im Salinargebirge bei mono- und multizyklischer Belastung. PhD thesis, Technische Universität Clausthal, Clausthal-Zellerfeld, Germany
- Leverett M (1941) Capillary behavior in porous solids. *Trans AIME* 142(01):152–169
- Lux K, Lerche S, Dyogtyev O (2018) Intense damage processes in salt rock—a new approach for laboratory investigations, physical modelling and numerical simulation. In: *Mechanical Behavior of Salt IX*, Hannover, Germany, pp 12–14
- McTigue DF (1986) Thermoelastic response of fluid-saturated porous rock. *J Geophys Res Solid Earth* 91(B9):9533–9542. <https://doi.org/10.1029/JB091iB09p09533>
- McTigue DF, Nowak EJ (1987) Brine transport studies in the bedded salt of the Waste Isolation Pilot Plant (WIPP). Tech. Rep. SAND-87-1274C, Sandia National Laboratories, Albuquerque, NM (USA)
- Pruess K, Oldenburg C, Moridis G (2012) TOUGH2 User's guide, version 2.0, report lbnl-43134
- Rutqvist J, Wu YS, Tsang CF, Bodvarsson G (2002) A modeling approach for analysis of coupled multiphase fluid flow, heat transfer, and deformation in fractured porous rock. *Int J Rock Mech Min Sci* 39(4):429–442. [https://doi.org/10.1016/S1365-1609\(02\)00022-9](https://doi.org/10.1016/S1365-1609(02)00022-9)
- Stormont J (1997) In situ gas permeability measurements to delineate damage in rock salt. *Int J Rock Mech Min Sci* 34(7):1055–1064. [https://doi.org/10.1016/S1365-1609\(97\)90199-4](https://doi.org/10.1016/S1365-1609(97)90199-4)
- Stormont J, Daemen J, Desai C (1992) Prediction of dilation and permeability changes in rock salt. *Int J Numer Anal Meth Geomech* 16(8):545–569
- Sweet J, McCreight J (1983) Thermal conductivity of rock salt and other geologic materials from the site of the proposed waste isolation pilot plant. In: *Thermal Conductivity* 16. Springer, p 61–78
- Tounsi H, Rutqvist J, Hu M, Wolters R (2023) Numerical investigation of heating and cooling-induced damage and brine migration in geologic rock salt: Insights from coupled THM modeling of a controlled block scale experiment. *Comput Geotech* 154(105):161. <https://doi.org/10.1016/j.compgeo.2022.105161>
- Winterle J, Ofoegbu G, Pabalan R, Manepally C, Mintz T, Percy E, Fedors R (2012) Geologic disposal of high-level radioactive waste in salt formations. Tech. Rep. NRC-02-07-006, US Nuclear Regulatory Commission
- Wolters R (2014) Thermisch-hydraulisch-mechanisch gekoppelte Analysen zum Tragverhalten von Kavernen im Salinargebirge vor dem Hintergrund der Energieträgerspeicherung und der Abfallentsorgung: ein Beitrag zur Analyse von Gefügeschädigungsprozessen und Abdichtungsfunktion des Salinargebirges im Umfeld untertätiger Hohlräume. PhD thesis, Technische Universität Clausthal, Clausthal-Zellerfeld, Germany
- Wolters R, Lux KH, Düsterloh U (2012) Evaluation of rock salt barriers with respect to tightness: influence of thermomechanical damage, fluid infiltration and sealing/healing. *Mechanical behaviour of Salt VII*. CRC Press, pp 439–448

Publisher's Note Springer Nature remains neutral with regard to jurisdictional claims in published maps and institutional affiliations.